nature materials

LETTERS

PUBLISHED ONLINE: 17 NOVEMBER 2013 | DOI: 10.1038/NMAT3806

A silicon carbide room-temperature single-photon source

S. Castelletto[1]*, B. C. Johnson[2,3], V. Ivády[4,5], N. Stavrias[6], T. Umeda[7], A. Gali[4,8] and T. Ohshima[3]

Over the past few years, single-photon generation has been realized in numerous systems: single molecules[1], quantum dots[2–4], diamond colour centres[5] and others[6]. The generation and detection of single photons play a central role in the experimental foundation of quantum mechanics[7] and measurement theory[8]. An efficient and high-quality single-photon source is needed to implement quantum key distribution, quantum repeaters and photonic quantum information processing[9]. Here we report the identification and formation of ultrabright, room-temperature, photostable single-photon sources in a device-friendly material, silicon carbide (SiC). The source is composed of an intrinsic defect, known as the carbon antisite–vacancy pair, created by carefully optimized electron irradiation and annealing of ultrapure SiC. An extreme brightness (2×10^6 counts s^{-1}) resulting from polarization rules and a high quantum efficiency is obtained in the bulk without resorting to the use of a cavity or plasmonic structure. This may benefit future integrated quantum photonic devices[9].

Silicon carbide is an important wide-bandgap semiconductor for high-power electronics and high-temperature applications, and is a key material for next-generation photonic[10] and electronic devices[11]. As such, SiC has well-established growth and device engineering protocols[12], and 3-inch ultrapure wafers are now commercially available. This has allowed the development of a mature platform for nanofabrication and high-Q photonic crystal cavities, reported for a spectral region from 550 to 1,450 nm (ref. 10) as well as microdisc resonators[13] for cavity opto-mechanical applications. In addition, SiC is also biocompatible, especially with blood, and SiC nanoparticles (quantum dots) have been employed as fluorescent biological labels in cell imaging[14,15].

Recently, it has been indicated[16–20] that SiC could harbour defects that may be employed as solid-state 'qubits'. The existence of such defects in a device-friendly material is extremely fortuitous and holds great promise for the future implementation of scalable quantum processors[17,21]. Ensembles of candidate optically active defects, having the net angular momentum (or spin) required to act as 'qubits' operating at room temperature, have already been identified in SiC (refs 18–20). Their optically detected magnetic resonance has a lower visibility compared with the nitrogen–vacancy centre in diamond[5]. However, the richness of possible defects in the various polytypes of SiC (ref. 20) will enable further studies and discoveries. At present, a major challenge before the future deployment of this material in the field of quantum technologies is to identify and form isolated defects.

In this work, we present, to the best of our knowledge, the first observation and engineering of an isolated defect in SiC that exhibits single-photon emission. To isolate single defects and identify them, we irradiated ultrapure SiC with low electron fluences and we optimized the annealing temperature to increase/decrease the number of defects created from the single to the ensemble level. This approach allows the direct correlation between ensemble and single defects, otherwise often difficult. The emission rate of this single photon source is in the Mcounts s^{-1} regime, the brightest single photon in bulk material at room temperature. In comparison, Cr-related centres in bulk diamond yield a single-photon count rate of 0.7 Mcounts s^{-1} (ref. 22). Only Cr-related and silicon–vacancy centres in nanodiamonds can yield emission rates above 3–4 Mcounts s^{-1} (refs 23,24), although for the latter case enhancement of the spontaneous emission count rate arose from plasmonic effects due to a metal substrate. A maximum emission rate of 1–2 GHz for nitrogen–vacancy centres in nanodiamonds can be achieved using a solid immersion lens to enhance the collection efficiency although with higher pump powers the nitrogen–vacancy centre is prone to blinking[25]. The SiC single-photon source has several zero-phonon lines and so is expected to exhibit efficient cavity coupling at low temperatures. At present, the brightest solid-state single-photon sources are based on advanced fibre-coupled microcavity-InAs/GaAs-quantum dots, reaching gigahertz repetition rate single-photon emission at 4 K (ref. 26). Further development of single-photon emission in SiC nanoparticles is expected to provide similar rates. Our work together with the possibility of nanostructuring this material will pave the way for further studies on the spin and charge state of this defect as well as quantum emitters in this emerging material.

High-purity, semi-insulating 4H-SiC wafers were irradiated with high-energy electrons to different fluences to create defects and then annealed at various temperatures (see Methods for details). This method allows the creation of defect densities from the single isolated level to the ensemble level.

To identify the defect, ensemble room-temperature and low-temperature photoluminescence measurements were performed with 532 nm excitation on a sample irradiated to a fluence of 10^{17} e cm^{-2}. At 80 K the so-called AB lines[27] can clearly be observed with lines at $A_1 = 648.7$ nm, $A_2 = 651.8$ nm, $B_1 = 671.7$ nm,

[1]School of Aerospace, Mechanical and Manufacturing Engineering RMIT University, Melbourne, Victoria 3000, Australia, [2]Centre for Quantum Computation and Communication Technology, School of Physics, University of Melbourne, Victoria 3010, Australia, [3]SemiConductor Analysis and Radiation Effects Group, Japan Atomic Energy Agency, 1233 Watanuki, Takasaki, Gunma 370-1292, Japan, [4]Institute for Solid State Physics and Optics, Wigner Research Centre for Physics, Hungarian Academy of Sciences, Budapest, POB 49, H-1525, Hungary, [5]Department of Physics, Chemistry and Biology, Linköping University, SE-581 83 Linköping, Sweden, [6]School of Physics, University of Melbourne, Victoria 3010, Australia, [7]Graduate School of Library, Information and Media Studies, University of Tsukuba, Tsukuba 305-8550, Japan, [8]Department of Atomic Physics, Budapest University of Technology and Economics, Budafoki út 8, H-1111 Budapest, Hungary. *e-mail: stefania.castelletto@rmit.edu.au

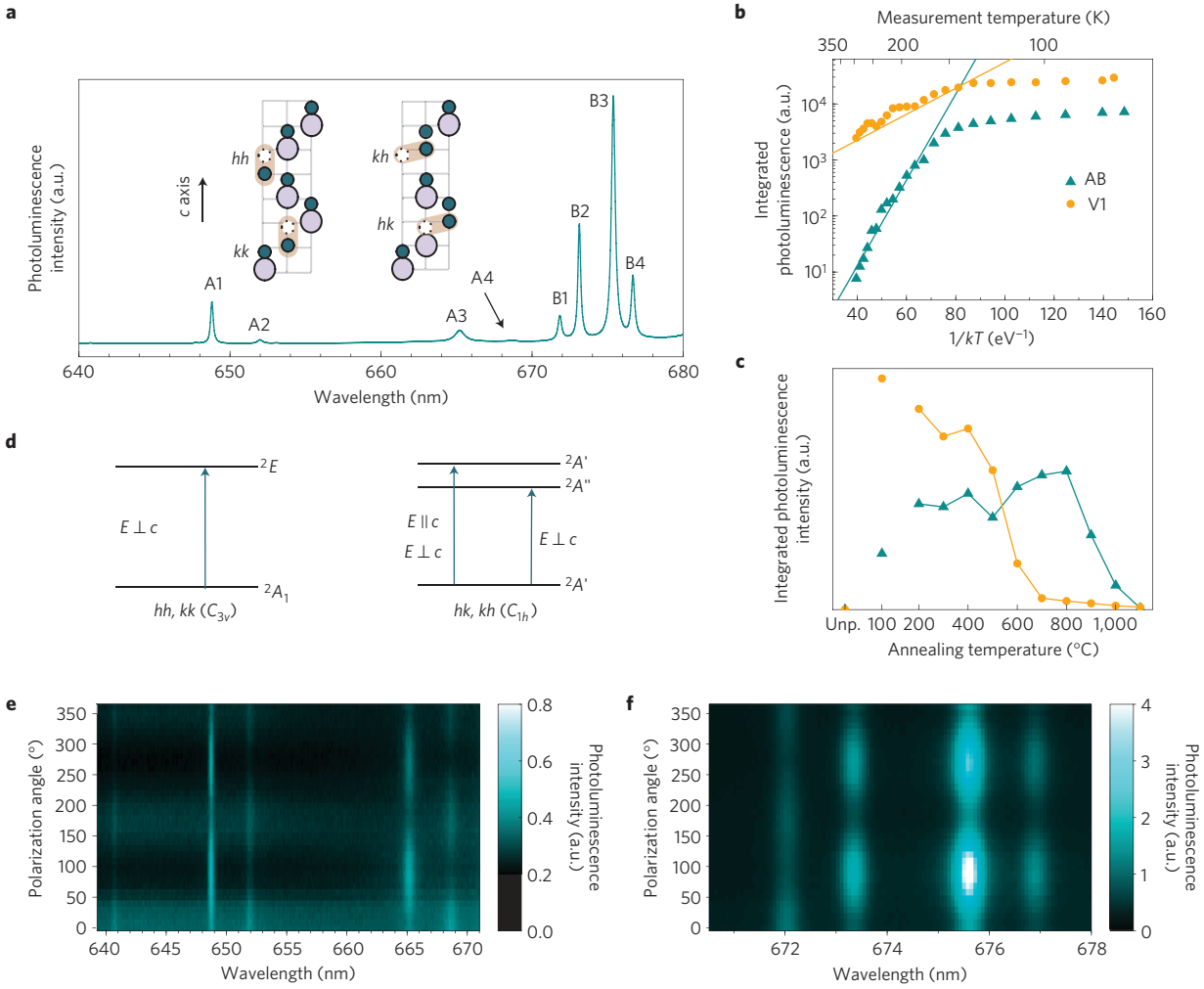

Figure 1 | Ensemble measurements of defects in electron-irradiated 4H-SiC. a, The AB photoluminescence lines observed in an electron-irradiated sample measured at 80 K. The proposed atomic structure of the defects $C_{Si}V_C$, giving rise to the photoluminescence, is shown in the (1120) plane with the *c* axis indicated in the inset (small and large circles represent C and Si atoms; the small open circles are vacancies). The carbon antisite–vacancy pair has four possible configurations in 4H-SiC: *hh*/*kk* axial configurations with C_{3v} symmetry, and *hk*/*kh* basal plane configurations with C_{1h} symmetry. *h* and *k* denote the hexagonal and cubic sites in the lattice, respectively. **b**,**c**, The temperature dependence of the AB and V1 photoluminescence lines (**b**) and, their annealing temperature dependence (**c**). **d**, Schematic diagram of the ground-state electronic structure of axial and basal plane configurations of the positively charged carbon antisite–vacancy defect. The symmetry labels of the defect states are depicted for each configuration. Arrows represent the feasible optical transitions with the corresponding polarization of light. **e**,**f**, The emission polarization dependence of the AB lines with the excitation beam perpendicular to the *c* axis and the polarization angle θ, with $\theta = 0$ parallel to the *c* axis. Unp., unprocessed.

$B_2 = 673.0$ nm, $B_3 = 675.2$ nm and $B_4 = 676.5$ nm, as indicated in Fig. 1a. These lines arise from the carbon antisite–vacancy pair defect, $C_{Si}V_C$ (ref. 28). We also resolve two additional peaks at $A_3 = 665.1$ nm and $A_4 = 668.5$ nm, which we assign to the same defect. The atomistic model of the $C_{Si}V_C$ with its four possible cubic or hexagonal orientations is shown in the inset of Fig. 1a.

A study on the effect of the measurement and annealing temperature on the AB lines (Fig. 1b,c) revealed the onset of thermal quenching at around 150 K and the enhancement of AB lines on annealing up to 800 °C. These measurements are compared to the silicon–vacancy defect, V_{Si} (ref. 29), which gives rise to the V1/V2 photoluminescence lines at 861.5 and 916.3 nm, respectively (see details in Supplementary Information). Here it is observed that the AB lines grow at the expense of V1. At the temperature at which the AB lines are optimized the V1/V2 system is almost absent. Such behaviour is supported by *ab initio* calculations where it has been shown that the energy barrier to formation of $C_{Si}V_C$ from V_{Si} is small and is promoted by an increase in the annealing temperature[30]. As will be shown, this has a large positive impact on the photostability of the $C_{Si}V_C$ at the single-defect level.

Ab initio supercell calculations on the $C_{Si}V_C$ defect in 4H-SiC in conjunction with group theory were employed to describe the AB photoluminescence spectra (see Supplementary Information).

A schematic of the electronic structure for both axial (*hh* and *kk*) and basal plane (*hk* and *kh*) configurations is shown in Fig. 1d. These levels arise in the bandgap owing to the dangling bonds of the carbon antisite as well as of the Si atoms nearest to the vacancy. In the axial configurations (C_{3v} symmetry), the lowest level has $^2A_1$ symmetry whereas the higher one has doubly degenerate ^2E symmetry. In the basal-plane configurations, the double-degenerate *E*-state splits owing to its lower C_{1h} symmetry.

Our *ab initio* calculations indicate that the neutral $C_{Si}V_C$ pair does not have photoluminescence in the visible, in contrast to the previous assignment[27]. Thus, our working model is the positively charged $C_{Si}V_C$ pair with predicted visible photoluminescence. In the ground state, only the lowest defect level is occupied by a single

electron, forming a totally symmetric state. The ^2E excited state of the axial configurations is subject to Jahn–Teller distortion whereas the basal configurations have *per se* C_{1h} symmetry. Thus, all of the configurations may have low symmetry in their excited state, and the resulting many-body wave functions could have either $^2A'$ or $^2A''$ symmetry. The latter may partially borrow the character of the ground state owing to sharing the same symmetry. The eight AB photoluminescence lines in 4H-SiC can naturally account for the four ground-state configurations where each possesses two zero-phonon lines. It was indeed shown that B_1 and B_3 lines are the higher excited states of B_2 and B_4 counterparts [27] separated by about 4 meV. A_1 and A_2 can naturally be grouped as well as the newly found A_3 and A_4 states, as they are separated by about the same energy as B_1 and B_3, or B_2 and B_4.

All of the configurations can be efficiently excited by $E \perp c$ light whereas $E \parallel c$ light excites configurations only to the A' excited state that partially shows the character of the ground state (Fig. 1d). Decay from the excited state can be more complicated than the optical excitation process. Direct recombination from the A'' or A' excited states to the A'' (or A_1) ground state is possible with the same polarization dependence as in the absorption process. However, non-radiative decay from the ^2E-like excited state may occur through a ^4E-like shelving state with the aid of a spin–orbit interaction and vibrations. From the *ab initio* calculations we conclude that only the single electron occupies the defect levels in the gap in the positively charged defect; thus, a ^4E-like shelving state may form with a hole left in the valence band edge whereas the A_1 level and the split E level are occupied by a single electron.

The emission polarization of the $C_{Si}V_C$ lines at 80 K is shown in Fig. 1e,f. Here, $\theta = 0$ corresponds to polarization parallel to the c axis. We find that the lowest excitations of the two configurations (A_2 and A_4) are partially $E \parallel c$ polarized whereas their higher energy counterparts, A_1 and A_3, are dominantly $E \perp c$ polarized. The other two configurations with the lowest energy (B_2 and B_4) are also dominantly $E \perp c$ polarized. However, only B_1 shows partial parallel $E \parallel c$ polarization, whereas B_3 is again dominantly $E \perp c$ polarized. This implies that the ground-state character has only a minute contribution to the A' excited state in the B_4 defect. Our *ab initio* calculations tentatively associate A_2, A_4, B_2 and B_4 lines with hh, hk, kk and kh configurations, respectively.

To isolate single bright defect centres we performed photoluminescence raster scans on samples irradiated with a low electron fluence (1×10^{13} e cm^{-2}) using room-temperature confocal microscopy. Typical maps are shown in Fig. 2a,b obtained by exciting either with 532 or 660 nm light in the same area in the sample. The observed centres are found 1–1.5 μm below the surface (see Supplementary Information), which is amenable for the integration of these defects into on-chip optical waveguides in photonic circuits. The number of centres in these maps is shown in Fig. 2c as a function of their spatial diameter at half-maximum. These are compared with an untreated sample excited with the 660 nm laser that also contains a number of optically active centres but at a much reduced density. It is clear that the 532 nm excitation allows a larger number of centres to be addressed with both A and B lines being excited. The 660 nm laser will mostly excite only the B lines. Furthermore, although these sources are present in these particular untreated samples, irradiation and annealing significantly increase their density (Fig. 2d; see Supplementary Information) similar to the ensemble measurements presented above.

Photoluminescence spectra corresponding to the bright spots in the confocal maps, when excited using either 660 or 532 nm are shown in Fig. 2e. We find that all of the measured diffraction-limited spots of 300–400 nm in diameter have photoluminescence emission between 675–700 nm, when excited at 660 nm, or with broader emission with peaks from ∼660 to ∼705 nm when excited at 532 nm. Such emission corresponds to that of the room-temperature photoluminescence of the AB lines. We therefore identify the defect responsible for this emission with the $C_{Si}V_C$ pair. Some variability is observed in the photoluminescence peak position (see Supplementary Information) possibly as a result of addressing defects of a specific configuration.

To confirm that single defects are being addressed, a Hanbury Brown–Twiss (HBT) interferometer was used to verify single-photon emission. We observed that all defects exhibiting photoluminescence between 648–710 nm behaved as single photon sources; that is, the second-order photon correlation function at zero delay is $g^{(2)}(0) < 0$ (Fig. 2f). We analysed $g^{(2)}(\tau)$ at different excitation powers to study the photo-physics and the population dynamics from the ground state to the excited state.

To assess the properties of the single-photon emission accurately, the variability of their kinetics was established. Many photostable emitters (more than 100) were measured with the two different excitation wavelengths and analysed. From this analysis we deduced a typical excited-state lifetime of 1.2 ns, the existence of a metastable state with a short lifetime and a quantum efficiency of the defect of 70%. The shelving state is predicted by our theoretical model and is an intrinsic part of the centre's electronic structure. The observed short metastable-state lifetime can be due to effective scattering from the sub-states of the shelving state.

The saturation properties of the defects also exhibit a remarkable variability, with optical saturation powers observed between 0.2 and 3.3 mW and saturation count rates found from 2.5×10^5 counts s^{-1} to the maximum observed of 2×10^6 counts s^{-1}. This variability is associated with the metastable-state lifetime variation. The high quantum efficiency and the most efficient excitation of axial defects (excitation orthogonal to the c axis) allows the maximum collection efficiency with the optical configuration of the confocal system used, yielding the high count rate measured for this defect.

We monitored the photoluminescence emission stability of these defects in a sample irradiated and annealed at 300 °C. It was observed that 45% of the emitters measured were stable over a long period of time. An example of such a single centre is shown in Fig. 3a along with its associated Gaussian count rate histogram in Fig. 3b. Interestingly, the remaining centres showed photoluminescence blinking with some eventually photo-bleaching, even if not permanently. Blinking centres in samples annealed at higher temperatures (500 °C) were almost absent even though the single-photon source density was greater. By annealing up to 800 °C, 65% of the emitters were stable for days at 532 nm excitation.

This suggests that the photostability may be compromised by the density of non-radiative pathways that are thermally unstable and annihilate on annealing. An emitter with on/off fluorescence, between two photoluminescence states, is shown in Fig. 3c,d. By measuring all on/off-time durations in a single trace, the corresponding probability of occurrence $P(\tau_{on,off})$ can be calculated. The distribution of the 'on' and 'off' times are plotted on a semi-logarithmic scale in Fig. 3e together with the fits. Both $P(\tau_{on})$ and $P(\tau_{off})$ show an exponential trend following the equation:

$$P(\tau_{on,off}) \propto \exp[-\tau/(\tau_{on,off})]$$

with the time constant τ_{on} usually much greater than τ_{off} (Fig. 3f) and very sensitive to the excitation power. This is in contrast to the more common power-law dependence usually observed for blinking. We attribute the observed blinking to either a photo-induced charge conversion of the addressed defect or to a charge exchange with other defects in close proximity, acting as charge traps or donors, probably induced by irradiation.

Samples annealed at higher temperature revealed a largely reduced number of blinking defects, indicating that the blinking can be controlled. In addition, the defects were more stable using 660 nm excitation.

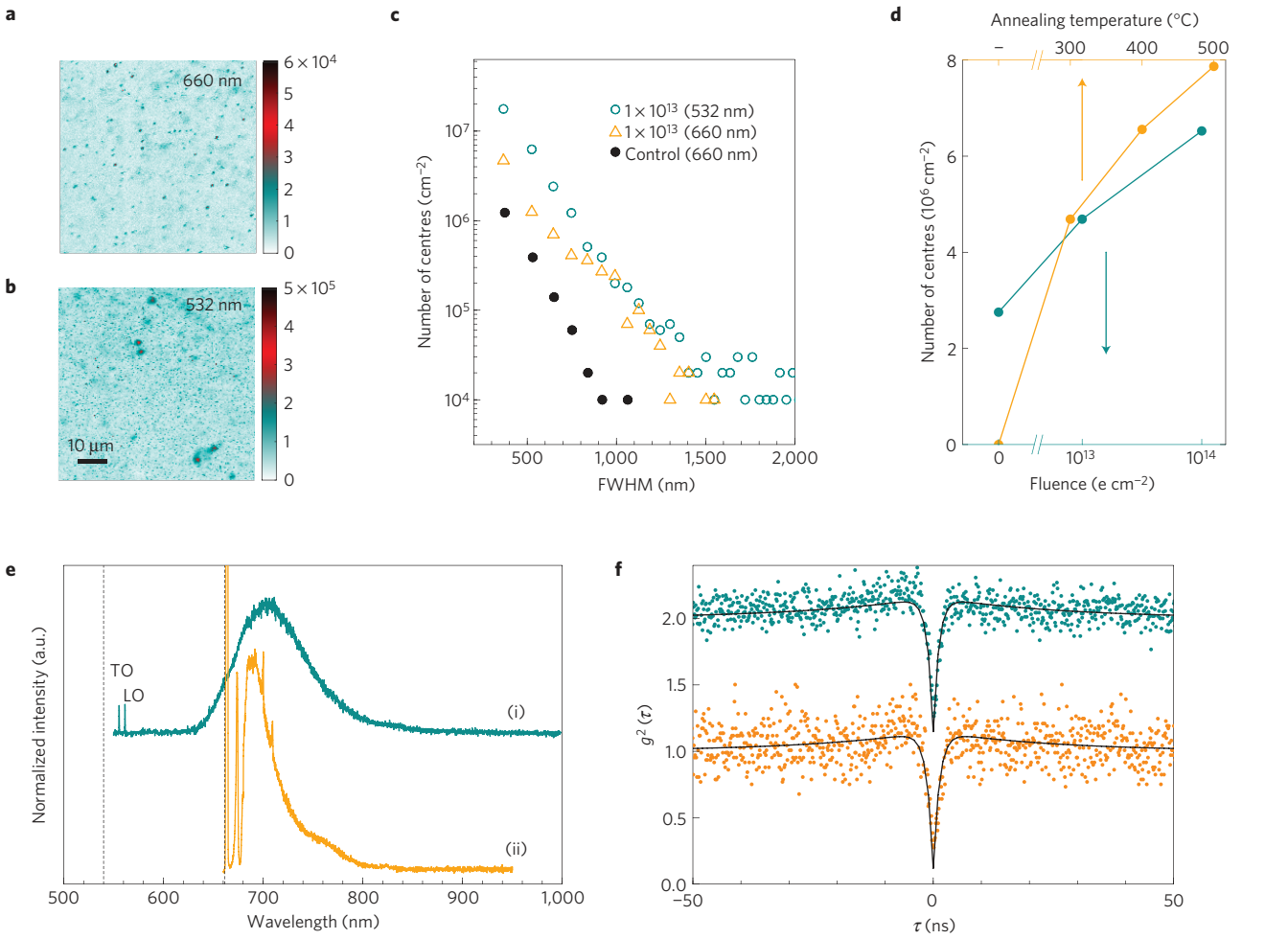

Figure 2 | Confocal microscopy of single-defect localization in 4H-SiC. a,**b**, Confocal maps of the low electron fluence sample excited with 660 nm (**a**) and 532 nm (**b**) lasers. The diffraction-limited spots all correspond to single-photon emitters. The map (**a**) has been scanned using a 10 nm full-width at half-maximum (FWHM) 694 nm filter. Note the difference in colour scale. **c**, Histogram of the number of centres observed as a function of the spatial FWHM measured and counted from **a**,**b**. The histogram from a confocal map of an unprocessed sample is also shown (black filled circles), indicating a clear increase in the defect density after irradiation and annealing at 300 °C. **d**, The number of diffraction-limited optical centres measured from single defects as a function of the annealing temperature (top axis) and fluence (bottom axis). **e**, Normalized room-temperature photoluminescence of a single-photon source in the irradiated sample excited with 532 nm (i) and 660 nm (ii) lasers. The laser wavelengths are indicated by the dashed lines. The transverse and longitudinal optic Raman modes (TO, LO) are also indicated. **f**, The corresponding anti-bunching curves for **e** (i) and (ii).

Our atomistic model of the defect (see Supplementary Information) indicates that the nature of the shelving state may also be responsible for the blinking properties (for example, a nearby defect can effectively capture the loosely bound hole and hinder the luminescence). This is consistent with our observation that with the appropriate anneal the defect density is reduced and blinking is minimized. Blinking may also arise in our working model by the fact that if the defect was originally neutral then it can be efficiently ionized to the luminescent positively charge state; in this case, the electrons should be continuously pumped to the conduction band to maintain the luminescence; 660 nm excitation can ionize the neutral defect but it has less probability to ionize the defect further (doubly positive charge state), and thus it can show greater photostability than with 532 nm excitation. Given that the blinking can be controlled with laser power, wavelength or annealing, we conclude that blinking is not an intrinsic property of the defect.

In our working model the spin state is 1/2 for the positively charged $C_{Si}V_C$ defect. Clearly, further theoretical modelling and experiments are required to determine whether this charge state could have an optically detected magnetic resonance (ODMR). We note that our working model indicates a relatively low ODMR signal because its metastable shelving state has low symmetry with a strong mixture of $m_S = \pm 1/2$ and $m_S = \pm 3/2$ substates. With a small magnetic field the ground state can be split but it is not understood whether different decay rates to these two states will be different enough to observe ODMR. The metastable state however might be used for spin readout. We further note that the spin-1/2 $C_{Si}V_C$ defect may cause decoherence of silicon–vacancy spins where the silicon–vacancy is created with optically polarizable spins together with the $C_{Si}V_C$ defect. The $C_{Si}V_C$ spin may communicate with silicon–vacancy spins through dipole–dipole interactions affecting the coherence time of those spins[20,29]. Thus, the manipulation of the ground and excited states of the $C_{Si}V_C$ defect at the single-defect level might be useful in the manipulation of other optically addressable nearby spins.

In conclusion, this ultrabright single-photon emitter working at room temperature provides a new building block in SiC-based opto-electronic devices and future integrated quantum photonics[9]. We envisage that SiC will constitute an ideal platform for future integrated photonic circuits comprising photonic cavities and waveguides, under fabrication at present. Our

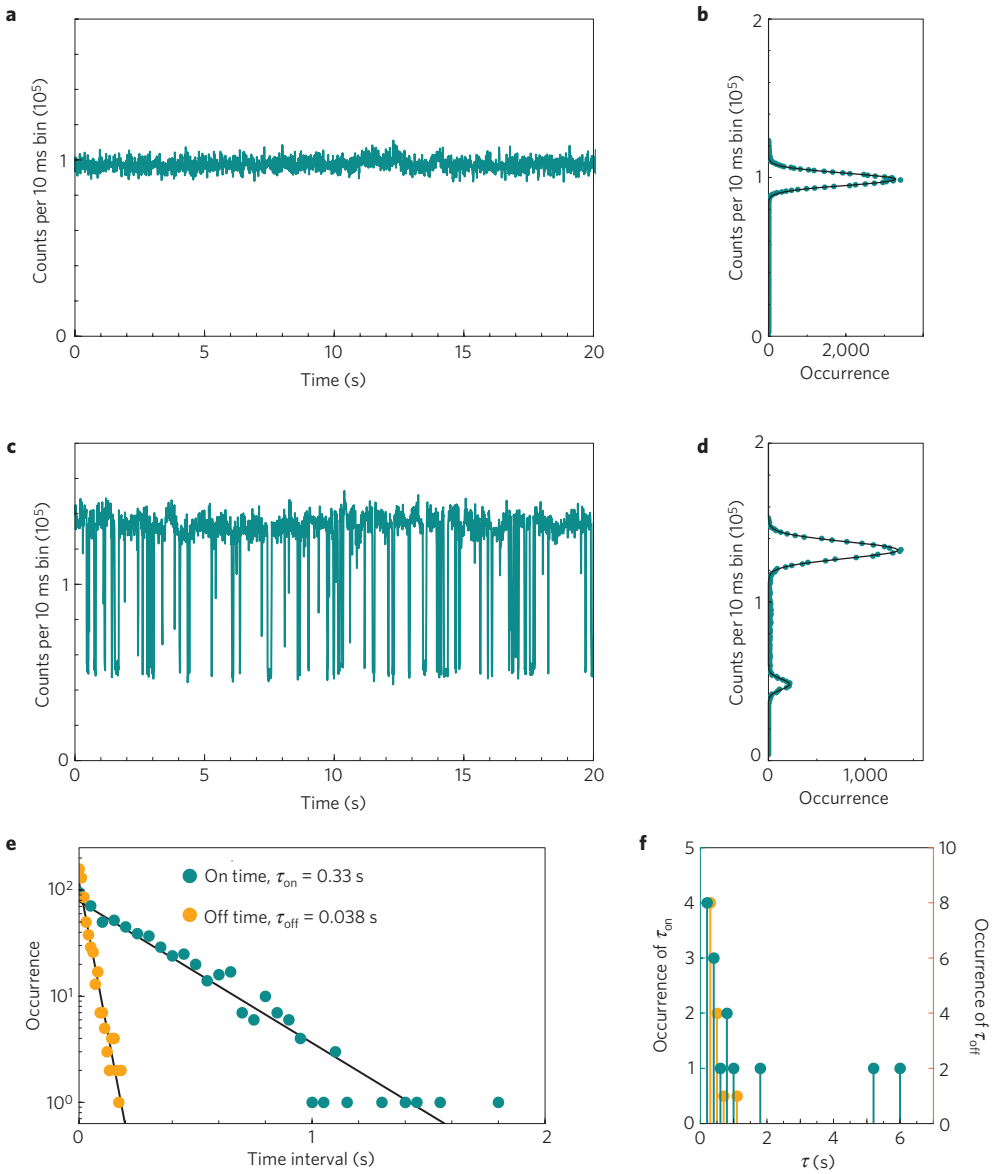

Figure 3 | Photo-stability of single-photon sources in SiC. a,**b**, A 20 s fragment of a photoluminescence time-trace sampled into 10 ms bins from a stable single-photon source (**a**) with its corresponding count rate histogram (**b**). **c**,**d**, A similar time trace is shown for a blinking centre. **e**, The on and off times of **c** are shown on a semi-logarithmic scale. **f**, Histogram of the measured τ_{on} and τ_{off} of the 55 emitters analysed. 45% of the emitters in this sample were stable and did not show blinking behaviour.

defect assignment yields good agreement with observations. The counterparts to this intrinsic defect can exist in other SiC polytypes and may also possess single-photon emission characteristics. The incorporation of these bright defects in SiC nanoparticles and SiC quantum dots could provide an exciting opportunity for biological imaging and microscopy.

Further optimization of the defect formation and excitation is expected to improve the photostability, its brightness and understanding of its properties. Electrical excitation of the centre is also a very realistic possibility that may result in SiC light-emitting diodes with active quantum systems[31].

Methods

Sample preparation. The material under study is high-purity semi-insulating 4H-SiC purchased from CREE. According to the manufacturer, the as-received samples contained B (10^{14} cm^{-3}), C interstitials (10^{14} cm^{-3}) and N ($<10^{14}$ cm^{-3}).

Samples were irradiated with 2 MeV electrons to fluences of 1×10^{13}, 1×10^{15} and 1×10^{17} e cm^{-2} at a flux of 2.82×10^{12} cm^{-2} s^{-1}. The samples were held at temperatures below 80 °C during irradiation in a nitrogen ambient to inhibit Frenkel pair annihilation and reduce the possibility of contamination. After irradiation, anneals between 200 and 1,100 °C in an Ar ambient for 30 min were carried out. Previous ensemble electron spin resonance measurements were also used to optimize anneals to enhance particular defects[32]. An unprocessed sample from the same wafer was also characterized to establish the effectiveness of the irradiation procedure employed.

Photoluminescence and photon correlation measurements. A HBT interferometer was used to identify optically active single defects and measure the time correlation of the centre emission. In the confocal microscope the samples were excited using a 0.2–1.5 mW continuous-wave laser operating at 532 nm (Coherent, model: Compass 315 M-100) and a continuous diode laser operating at 665 nm. The laser was focused onto the sample using a ×100 infinity-corrected oil-immersion objective lens with a NA of 1.4 and the luminescence was collected confocally through a 50 μm pinhole. A spectrometer (Princeton Instruments Acton 2500i, Acton) with a cooled CCD (charge-coupled device) (Camera Pixis 100 model: 7,515–0,001 Princeton Instruments) was used to characterize the luminescence and a HBT interferometer with single-photon-sensitive avalanche photodiodes (Perkin Elmer SPCM-AQR 14) was used to measure the photon statistics. Photon counting and correlation was carried out using a time-correlated single-photon-counting module (PicoHarp 300, PicoQuant GmbH).

The 4H-SiC samples were mounted on a piezoelectric *XYZ* stage allowing $100 \times 100\,\mu m^2$ scans. The unwanted residual laser line was eliminated by a 660-nm long-pass filter. A filter with 694 ± 10 nm was placed in front of the HBT interferometer to observe single photons during the 660-nm laser excitation. The spectroscopy was done using only a long-pass filter. All of the single-photon/single-defect measurements were performed at room temperature.

A Renishaw MicroRaman Spectrometer equipped with a Linkam stage for temperature control was used for the ensemble photoluminescence measurements. A 532-nm laser was directed through a ×20 long-working-distance objective with a 0.4 NA onto the sample. The laser power at the sample was approximately 0.5 mW. The spectrometer has a working distance of 0.25 m and uses an 8 μm slit and a 1,200 g mm^{-1} grating. The detector is a fan-cooled Si CCD.

Atomistic simulations. Theoretical calculations were carried out using density functional theory and group theory. A 576-atom supercell with Γ-point sampling of the Brillouin zone was used in the supercell calculations on the $C_{Si}V_C$ defects in 4H-SiC. A Γ-point calculation is sufficient to provide convergent charge density and enabled us to study the degeneracy of the defect levels. We applied HSE06 hybrid density functional theory that is able to reproduce the experimental bandgap of 4H-SiC (≈3.2 eV) and defect levels in the fundamental bandgap[33,34]. We note that we were able to identify the electron paramagnetic spectrum of the negatively charged and positively charged $C_{Si}V_C$ pair using supercell density functional theory methods in refs 32,35.

Received 15 December 2012; accepted 7 October 2013; published online 17 November 2013

References

1. Basché, T., Moerner, W. E., Orrit, M. & Talon, H. Photon anti-bunching in the fluorescence of a single dye molecule trapped in a solid. *Phys. Rev. Lett.* **69,** 1516–1519 (1992).
2. Michler, P. *et al.* Quantum correlation among photons from a single quantum dot at room temperature. *Nature* **406,** 968–970 (2000).
3. Santori, C., Fattal, D., Vuckovic, J., Solomon, G. S. & Yamamoto, Y. Indistinguishable photons from a single-photon device. *Nature* **419,** 594–597 (2002).
4. Shields, A. J. Semiconductor quantum light sources. *Nature Photon.* **1,** 215–223 (2007).
5. Kurtsiefer, C., Mayer, S., Zarda, P. & Weinfurter, H. Stable solid-state source of single photons. *Phys. Rev. Lett.* **85,** 290–293 (2000).
6. Kolesov, R. *et al.* Optical detection of a single rare-earth ion in a crystal. *Nature Commun.* **3,** 1029 (2012).
7. Peruzzo, A., Shadbolt, P., Brunner, N., Popescu, S. & O'Brien, J. L. A quantum delayed-choice experiment. *Science* **338,** 634–637 (2012).
8. Lundeen, J. S., Sutherland, B., Patel, A., Stewart, C. & Bamber, C. Direct measurement of the quantum wavefunction. *Nature* **474,** 188–191 (2011).
9. Politi, A., Matthews, J. C. F. & O'Brien, J. L. Shor's quantum factoring algorithm on a photonic chip. *Science* **325,** 1221 (2009).
10. Yamada, S., Song, B-S., Asano, T. & Noda, S. Silicon carbide-based photonic crystal nanocavities for ultra-broadband operation from infrared to visible wavelengths. *Appl. Phys. Lett.* **99,** 201102 (2011).
11. Madar, R. Materials science: Silicon carbide in contention. *Nature* **430,** 974–975 (2004).
12. Nakamur, D. *et al.* Ultrahigh-quality silicon carbide single crystals. *Nature* **430,** 1009–1012 (2004).
13. Lu, X., Lee, J. Y., Feng, P. X-L. & Lin, Q. Silicon carbide microdisk resonator. *Opt. Lett.* **38,** 1304–1306 (2013).
14. Fan, J. *et al.* 3C–SiC nanocrystals as fluorescent biological labels. *Small* **4,** 1058–1062 (2008).
15. Beke, D. *et al.* Silicon carbide quantum dots for bioimaging. *J. Mater. Res.* **28,** 205–209 (2013).
16. Gali, A. Excitation spectrum of point defects in semiconductors studied by time-dependent density functional theory. *J. Mater. Res.* **27,** 897–909 (2012).
17. Weber, J. R. *et al.* Quantum computing with defects. *Proc. Natl Acad. Sci. USA* **107,** 8513–8518 (2010).
18. Koehl, W. F., Buckley, B. B., Heremans, F. J., Calusine, G. & Awschalow, D. D. Room temperature coherent control of defect spin qubits in silicon carbide. *Nature* **479,** 84–87 (2011).
19. Baranov, P. G. *et al.* Silicon vacancy in SiC as a promising quantum system for single-defect and single-photon spectroscopy. *Phys. Rev. B* **83,** 125203 (2011).
20. Falk, A. L. *et al.* Polytype control of spin qubits in silicon carbide. *Nature Commun.* **4,** 1819 (2013).
21. DiVincenzo, D. Quantum bits: Better than excellent. *Nature Mater.* **9,** 468–469 (2010).
22. Aharonovich, I. *et al.* Chromium single-photon emitters in diamond fabricated by ion implantation. *Phys. Rev. B* **81,** 121201 (2010).
23. Aharonovich, I. *et al.* Two-level ultrabright single photon emission from diamond nanocrystals. *Nano Lett.* **9,** 3191–3195 (2009).
24. Neu, E. *et al.* Single photon emission from silicon-vacancy colour centres in chemical vapour deposition nano-diamonds on iridium. *New J. Phys.* **13,** 025012 (2011).
25. Schröder, T., Gädeke, F., Banholzer, M. J. & Benson, O. Ultrabright and efficient single-photon generation based on nitrogen-vacancy centres in nanodiamonds on a solid immersion lens. *New J. Phys.* **13,** 055017 (2011).
26. Ates, S. *et al.* Improving the performance of bright quantum dot single photon sources using temporal filtering via amplitude modulation. *Sci. Rep.* **3,** 1397 (2013).
27. Steeds, J. W. Photoluminescence study of the carbon antisite-vacancy pair in 4H-and 6H–SiC. *Phys. Rev. B* **80,** 245202 (2009).
28. Steeds, J. *et al.* Transmission electron microscope radiation damage of 4H and 6H SiC studied by photoluminescence spectroscopy. *Diamond Relat. Mater.* **11,** 1923–1945 (2002).
29. Soltamov, V. A., Soltamova, A. A., Baranov, P. G. & Proskuryakov, I. I. Room temperature coherent spin alignment of silicon vacancies in 4H-and 6H–SiC. *Phys. Rev. Lett.* **108,** 226402 (2012).
30. Bockstedte, M., Mattausch, A. & Pankratov, O. *Ab initio* study of the annealing of vacancies and interstitials in cubic SiC: Vacancy-interstitial recombination and aggregation of carbon interstitials. *Phys. Rev. B* **69,** 235202 (2004).
31. Fuchs, F. *et al.* Silicon carbide light-emitting diode as a prospective room temperature source for single photons. *Sci. Rep.* **3,** 1637 (2013).
32. Umeda, T. *et al.* Identification of the carbon antisite-vacancy pair in 4H-SiC. *Phys. Rev. Lett.* **96,** 145501 (2006).
33. Deák, P., Aradi, B., Frauenheim, T., Janzén, E. & Gali, A. Accurate defect levels obtained from the HSE06 range-separated hybrid functional. *Phys. Rev. B* **81,** 153203 (2010).
34. Ivády, V., Gällström, A., Son, N. T., Janzén, E. & Gali, A. Asymmetric split-vacancy defects in SiC polytypes: A combined theoretical and electron spin resonance study. *Phys. Rev. Lett.* **107,** 195501 (2011).
35. Umeda, T. *et al.* Identification of positively charged carbon antisite-vacancy pairs in 4H-SiC. *Phys. Rev. B* **75,** 245202 (2007).

Acknowledgements

S.C. acknowledges partial financial support from the Australian Research Council, Centre of Excellence Engineered Quantum Systems (CE110001013). B.C.J. acknowledges financial support from the Japanese Society for the Promotion of Science (JSPS; Grant-in-aid for Scientific Research, 22.00802) and the Australian Research Council Centre for Quantum Computation and Communication Technology (CE110001027). This study is also partially supported by the Ministry of Education, Science, Sports and Culture, Grant-in-Aid for Challenging Exploratory Research, 2012, 24656025. A.G. acknowledges the EU FP7 Grant No. 270197 (DIAMANT), the Hungarian OTKA Grant Nos K101819 and K106114 and the support from the Knut and Alice Wallenberg Foundation.

Author contributions

S.C. and B.C.J. proposed the idea and the strategy for the experimental design and data analysis and wrote the paper. S.C. performed the optical single-photon characterization experiments. B.C.J. irradiated and annealed the samples and made the low-temperature photoluminescence measurements. N.S. performed some of the low-temperature photoluminescence measurements. S.C. and B.C.J. coordinated the experiments and analysed the data. V.I. and A.G. performed the theoretical model of the centre. S.C., B.C.J. and A.G. contributed to writing the manuscript. All authors discussed the results and commented on the manuscript.

Additional information

Supplementary information is available in the online version of the paper. Reprints and permissions information is available online at www.nature.com/reprints. Correspondence and requests for materials should be addressed to S.C.

Competing financial interests

The authors declare no competing financial interests.